Eur. Phys. J. B **16**, 223–231 (2000)

THE EUROPEAN PHYSICAL JOURNAL B

EDP Sciences

Solid-state interfacial reaction and asymmetric growth of amorphous interlayers in Ni/Nb multilayers. Molecular-dynamics simulation together with experiments

Q. Zhang[1], W.S. Lai[1], G.W. Yang[1], and B.X. Liu[1,2,a]

[1] Department of Materials Science and Engineering, Tsinghua University, Beijing 100084, P.R. China
[2] National Laboratory of Solid-State Microstructure, Nanjing University, Nanjing 210093, P.R. China

Received 7 June 1999 and Received in final form 12 January 2000

Abstract. An embedded-atom potential for the Ni-Nb system is constructed using physical properties obtained from first-principle calculations. Employing the potential, molecular-dynamics simulations are performed to study the interfacial reaction in Ni/Nb multilayers upon annealing at medium temperatures. The results show that a preset disordered interlayer, which is obtained by exchanging Ni and Nb atoms in the interfaces, may act as a nucleus of amorphous phase and is usually necessary for amorphization. It is found that the growth of the amorphous interlayer is in a planar mode and exhibits an asymmetric behavior due to a faster consumption of Ni than that of the Nb layer; this is also indeed observed experimentally. Moreover, performing a simulation with solid solution models, it is found that the Nb lattice can accommodate a large number of Ni atoms and still retain a crystalline structure, while a small amount of Nb atoms induce a spontaneous decay of the Ni lattice. Such differences in solid solubility is thought to be the physical origin of the asymmetric growth observed in experiments and simulations.

PACS. 64.70.Kb Solid-solid transitions – 82.20.Wt Computational modeling; simulation – 61.43.Dq Amorphous semiconductors, metals, and alloys

1 Introduction

The solid-state amorphization (SSA) in multilayers was first observed by Schwarz and Johnson in the Au-La system [1]. Since then some experiments have been performed in other binary metal systems to investigate their capability and behavior of SSA [2,3]. It has been considered that the glass-forming systems should have a negative heat of formation ΔH_{F} serving as a thermodynamic driving force for SSA. Besides, the possible crystallization of the equilibrium compound should be kinetically hindered [4]. To form a nucleus of a crystalline intermetallic compound, the atoms of both metal species are required to be rearranged both topologically and chemically, whereas the formation of an amorphous nucleus is far less restrictive in both aspects. The nucleation barrier of an amorphous phase is therefore less than that of intermetallic compounds, leading to the formation of an amorphous phase through interfacial reaction upon isothermal annealing at a low temperature for a short time [4].

It has been observed experimentally that the initial interfacial structure in the multilayers had a significant influence on the solid-state reaction. For instance, Clemens reported that in Ni/Ti multilayers, SSA could take place upon annealing when the interfacial layers were in a disordered state, and also that the interfacial reaction was completely suppressed if coherent interfaces emerged [3]. Vredenber *et al.* examined polycrystalline Ni/single crystal Zr (112) diffusion couples: for this case, it was found that amorphization could only take place after a disordered interlayer had been formed by ion beam at the interface [5]. These observations imply that a sharp interface may act as a nucleation barrier against interfacial reaction. Through thermodynamic analyses, several models have been proposed to explain the nucleation of amorphous phase. For example, Highmore assumed that two solid solutions, formed through exchanging two kinds of atoms at the interface, were precursors to the glassy phase [6]. Up-to-now however, the nucleation mechanism of the amorphous phase at an atomic scale has not been clear.

Besides, some carefully performed experiments revealed an asymmetric growth behavior in SSA. For instance, from a cross-sectional Ni/Zr bilayer sample Meng *et al.* observed that during the growth of the Ni-Zr amorphous interlayer a compound was first formed at the amorphous/Zr interface [7], implying the growing speed towards Zr was slower than that in the opposite direction. Direct experimental evidence of the asymmetric growth was reported by Schröder *et al.* in the Co/Zr system, *i.e.*

[a] e-mail: dmslbx@tsinghua.edu.cn

they observed that the amorphous interlayer grew by consuming Co and Zr with a quantity ratio of about 2:1 [8]. Recently, such an asymmetric growth phenomenon was also revealed by MD simulations in the Ni/Zr and Ni/Mo multilayers [9,10]. To obtain a clear understanding of the asymmetric behavior, more detailed investigations are required.

In this study, we conduct MD simulation to investigate the detailed mechanism of SSA in the Ni-Nb system, which is a typical glass-forming system with a heat of formation of −44 kJ/mol. To our knowledge, there is only one Ni-Nb potential, constructed by Kreuch and Hafner using a hybridized nearly-free-electron-tight-binding-bond (NFE-TBB) method. The method is based on first-principle calculations and various effective pair potentials should be derived for alloys with various compositions [11]. As the potential was not applicable for our study, we first constructed an n-body Ni-Nb potential based on the embedded-atom method (EAM) [12]. MD simulations were then performed with the constructed potential to reveal the detailed process of amorphization. We also conducted some solid-state interfacial reaction experiments to compare with the simulation results. Finally, we tried to clarify the physical origin of the asymmetric growth in SSA by simulation using solid solution models.

2 Construction of an n-body potential

The n-body potential was first developed by Daw and Baskes who proposed an approach named the embedded-atom method (EAM), which is based on density functional theory. This method has been used extensively for metals [12,13]. Subsequently, other researchers have presented other methods to construct n-body potentials [14,15]. In the EAM potential, the total energy of a system is designed to follow Rose's equation of state [16] in the fitting procedure. The physical properties away from the equilibrium state are therefore regarded as fitted in EAM and the potential for pure metals can directly be applied to metallic alloys. In this study, we adopt the analytic form proposed by Johnson *et al.* for bcc metals and the form developed by Cai *et al.* for fcc metals [17,18].

In the framework of the EAM theory, the total energy of the system of N atoms is described as

$$E_{\mathrm{tot}} = \sum_i F_i(\rho_i) + \sum_{i>j} \phi(r_{ij}), \tag{1}$$

$$\rho_i = \sum_{j(\neq i)} f(r_{ji}) \tag{2}$$

where E_{tot} is the total energy, $F_i(\rho_i)$ is the embedding energy, ρ_i is the total electron density at atom i due to all other atoms, $\varphi(r_{ij})$ is the pair potential between atoms i and j, $f(r_{ji})$, is the atom electron density for atom i contributed by atom j. In Johnson's bcc model and Cai's fcc model, the embedding functions $F(\rho)$ are actually quite similar except for an additional linear term proposed by Cai *et al.* This is

$$F(\rho) = -F_0\left[1 - \ln\left(\frac{\rho}{\rho_{\mathrm{e}}}\right)^n\right]\left(\frac{\rho}{\rho_{\mathrm{e}}}\right)^n + F_1\left(\frac{\rho}{\rho_{\mathrm{e}}}\right)\cdot \tag{3}$$

For the bcc model F_1 equals 0, while for the fcc model F_1 is an adjustable parameter. In the two models $F_0 = E_{\mathrm{c}} - E_\nu^{\mathrm{f}}$, where E_{c} and E_ν^{f} are the cohesive energy and vacancy formation energy, respectively. ρ_{e} represents the host electron density at equilibrium. It is thus convenient to combine the two models together for the Ni(fcc)-Nb(bcc) system. Since the embedding function $F(\rho)$ is universal and does not depend on the source of the host electron density, the electron density functions $f_{\mathrm{Ni}}(r)$ and $f_{\mathrm{Nb}}(r)$ and the embedding energy functions $F_{\mathrm{Ni}}(\rho)$ and $F_{\mathrm{Nb}}(\rho)$ are assumed to be transferable from two monatomic systems to one binary metal system, as are the pair potential functions $\varphi_{\mathrm{Ni-Ni}}(r)$ and $\varphi_{\mathrm{Nb-Nb}}(r)$. The electron-density scaling factor f_{e} is determined by the equation $f_{\mathrm{e}} = E_{\mathrm{c}}/\Omega$ (E_{c} is the cohesive energy and Ω is the atom volume) as pointed out by Johnson [19]. In Cai's original scheme, the cutoff distance is taken between the fifth- and sixth-neighbor distances. In our study, the r_{cut} of Ni is assumed to be between the second- and third-neighbor distances and is compatible with that for Nb. The parameters in the Ni potential should therefore be refitted by an optimization procedure. Although our present model, similar to the original format, includes no long range force, the major intrinsic properties can still be reproduced and the deduced equation of state is in good agreement with Rose's. The potential parameters for Nb-Nb interaction are adopted from Johnson's data. The remaining function that needs to be developed is the cross pair potential function $\varphi_{\mathrm{Ni-Nb}}(r)$, which is assumed as

$$\begin{aligned}\varphi(r) &= (r-c)^2(c_0 + c_1 r + c_2 r^2 + c_3 r^3 + c_4 r^4) \quad r \le c\\ &= 0 \qquad\qquad\qquad\qquad\qquad\qquad\quad r > c\cdot\end{aligned} \tag{4}$$

Because of the shortage of the experimental data for the equilibrium Ni-Nb alloy phases, the parameters in $\varphi_{\mathrm{Ni-Nb}}(r)$ are derived from some physical properties obtained with linear muffin-tin orbital (LMTO) calculations [20] for four Ni-Nb metastable crystalline phases, among which three have been observed in experiments [21,22]. The fitting results are listed in Table 1. Employing the derived Ni-Nb potential, the cohesive energies, the lattice constants and the bulk moduli are reproduced for the above mentioned four metastable crystalline phases and listed in Table 2. These are in good agreement with the values obtained from first-principle calculations. Moreover, the reproduced lattice constants of the equilibrium β−Ni_3Nb phase also agree well with the experimental values within an error of only 2% [23]. To test the dynamic properties, the melting point of the β-phase is calculated by MD simulation to be 1750 K, which is compatible with the experimental value of 1703 K [24]. For these alloy phases, Rose's equation of state can also be reproduced by the derived potential. In short, the constructed Ni-Nb potential is therefore believed to be of relevance in describing the atomic interactions for the system.

Table 1. The potential parameters for Ni-Nb.

	c(Å)	c_0	c_1	c_2	c_3	c_4
Ni-Nb	3.8	51.683 55	−69.797 8	34.291 2	−7.189 241	0.523 113

Table 2. The comparison of the physical properties derived from the constructed potential with those from LMTO calculation. Cohesive energy in eV/atom, lattice constant in Å (experimental values, for Ni_3Nb D019, $c/a = 1.60$; $NiNb_3$ D019, $c/a = 1.63$).

		$-E_c$		B		a		
System	Structure	LMTO[a]	this work	LMTO	this work	LMTO	Expt.	this work
Ni_3Nb	$D0_{19}$	5.586	5.470	2.57	2.20	2.637	2.53[b]	2.577
	$L1_2$	5.439	5.425	2.54	2.29	3.717		3.629
$NiNb_3$	$D0_{19}$	6.711	6.737	2.25	1.5	2.915	2.91[c]	2.891
	$L1_2$	6.724	6.738	2.23	1.5	4.124	4.11[c]	4.078

[a]Reference [20] [b]Reference [21] [c]Reference [22]

Table 3. The crystalline directions of the fcc Ni and bcc Nb set to be parallel to the x- and y-axes corresponding to various interfacial orientations in the various sandwich-models.

	Ni(fcc)			Nb(bcc)		
	(001)	(110)	(111)	(001)	(110)	(111)
x	[100]	$[\bar{1}10]$	$[\bar{1}10]$	[100]	[001]	$[1\bar{1}0]$
y	[010]	[001]	$[\bar{1}\bar{1}2]$	[010]	$[1\bar{1}0]$	$[\bar{1}\bar{1}2]$

3 Models and computation

The Nb-Ni-Nb sandwich models are constructed by stacking Ni and Nb atomic planes along the z-axis and the orientations of the atomic planes are indexed by their Miller indices, *e.g.* [8 (001) Ni] refers to a Ni lattice of fcc structure stacking by 8 (001) atomic planes, and [6 (111) Nb] stands for a Nb lattice of bcc structure stacking by 6 (111) atomic planes, etc. In each sandwich model, there are two Ni/Nb interfaces parallel to the x-y plane. Altogether 9 sandwich-models can be constructed by combining Ni (110), (100) and (111) planes with Nb (100), (110) and (111) planes. The orientations of the atomic planes in the x-y planes are set to preserve the symmetry of the crystalline planes across the boundary, and the respective orientations are listed in Table 3. The sizes of the Ni and Nb lattices in the x-y plane are chosen to be as close as possible. For details, readers are referred to our previous papers [9,10]. For the boundary conditions, in the z-direction a periodic condition is imposed, and two Nb lattices in the sandwich-models are therefore adhered together to form a united lattice. In the x- and y-directions, the larger dimension of the Ni and Nb lattices is adopted to set the periodic boundary conditions. Consequently, a sandwich-model represents the compositional modulated multilayers used in experimental studies.

We also construct Ni-Nb bilayer-models to study the detailed kinetics of SSA. The construction of the model is similar to that of the sandwich-models, except in the z-direction where a free boundary condition is adopted and therefore there is only one interface in the model.

Based on the potential, a molecular-dynamics (MD) simulation of solid-state reaction in the Ni-Nb system is conducted with a Parrinello-Rahman MD scheme [25]. The equations of motion are solved using a fourth-order predictor-corrector algorithm of Gear with a time step $t = 5 \times 10^{-15}$ s. Simulation starts by equilibrating the model at room temperature (27 °C) to reach an equilibrium configuration as an initial state. From the initial state, the temperature of the model is then gradually raised at a rate of 4×10^{13} K/s to a designed value in a range of 300 to 600 °C, at which isothermal annealing is performed. During annealing, if the average deviation from the assigned temperature is over 1 °C, a re-scaling of the velocities to the assigned temperature is executed after every 10 time steps.

The most direct and convenient way to describe a reaction process is by simply displaying graphically, the distribution of atoms at various times onto a projected plane, *e.g.* x-z plane. Quantitatively, the structural evolution during the solid-state reaction of the Ni-Nb multilayers or bilayer is monitored by the well-known pair-correlation function $g(r)$, through which the structure of a block material can be identified [26]. To represent the degrees of disorder in the atomic planes, *i.e.* the original crystal planes, the planar structure factor $S(k)$ [27] is evaluated at each time step. The planar structure factor $S = 1$ refers to an entirely ordered crystal while $S = 0$ corresponds to a completely disordered state. Furthermore, the density profiles of each species along the z-direction $\rho_\alpha(z)$ are calculated to indicate the local structural and compositional information of the models [28].

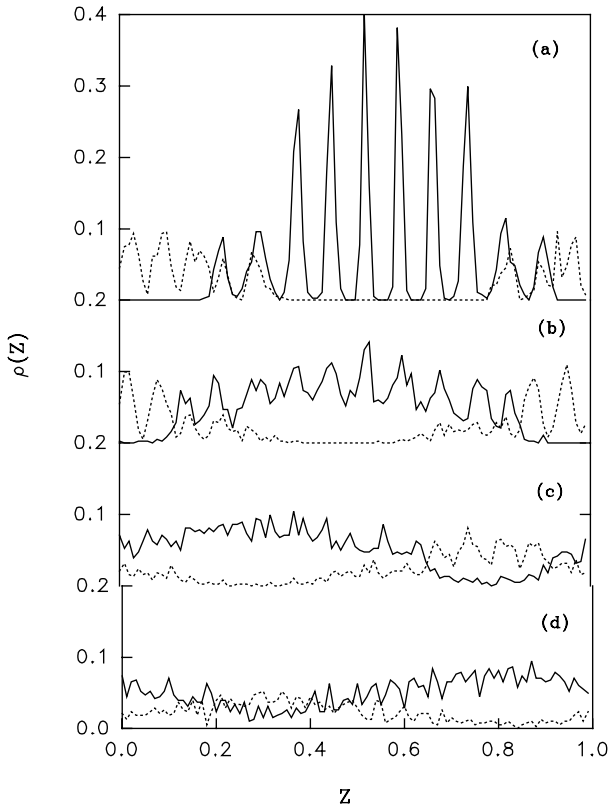

Fig. 1. The calculated density profiles, $\rho_\alpha(z)$, of each species along the z direction, perpendicular to the interface for the initial state and the states obtained at 500 °C annealing for 0.2, 0.5, 1.25 ns in the sandwich-model of [4 (001) Nb/8 (001) Ni/2 (001) Nb]. $\rho_{\rm Ni}(z)$ is represented by solid line and $\rho_{\rm Nb}(z)$ by dotted line. The ordinate is in arbitrary units. The shift of the peaks of $\rho_\alpha(z)$ is due to a variation of the computational block during annealing and the periodic boundary condition imposed in the z direction.

4 Simulation results

4.1 Sandwich-models

We first discuss the simulation results obtained with a sandwich-model [4 (001) Nb/8 (001) Ni/2 (001) Nb] after isothermal annealing at 500 °C. In this model, two interfaces are set between the atomic planes No. 4–5 and No. 12–13, respectively. After isothermal annealing at 500 °C for 80 000 MD time steps, *i.e.* 0.4 ns, little mutual diffusion can be visualized and the multilayers retain a crystalline structure, implying that such a sharp interface hinders the atomic diffusion and serves as a nucleation barrier.

To form a disordered interfacial structure of the multilayers as observed in experiments [3, 5], we adopt Highmore's assumption and randomly exchange Ni and Nb atoms in two interfaces. The concept of a long range order (LRO) parameter η is used to characterize quantitatively the amount of disorder created by exchanging atoms [29]. Values $\eta = 0$ and 1 correspond, respectively, to a complete chemical disorder and an entirely ordered crystalline state. In the sandwich model, 90 Ni and 90 Nb atoms are randomly exchanged in each interface leading to $\eta = 0$. The model is equilibrated at 27 °C for 25 ps to an initial state, which is then heated up to 500 °C for annealing. Figure 1 displays the changing of the density profiles, $\rho_\alpha(z)$, of each species along the z-direction upon isothermal annealing at 500 °C with increasing time steps. At the initial state, the Ni and Nb atomic planes retain good crystalline states and almost no alloying atoms have diffused into its partner lattice except the four interfacial atomic planes in which chemical disorder is already present. After isothermal annealing at 500 °C for 0.2 ns, more mutual diffusion takes place and all the Ni atomic planes become disordered, whereas four Nb atomic planes still remain in crystalline structures. With increasing annealing time, all the remaining crystalline Nb planes also become disordered and after 1.25 ns a uniform amorphous structure is obtained. Apparently, the extension of the disordered Ni-Nb layer is faster towards the Ni side than that directed to the Nb lattice, which is known as asymmetric growth of amorphous interlayer during SSA. To characterize the structural change during thermal annealing, four sets of partial and total pair-correlation functions are calculated at various time steps and are shown in Figure 2. One observes that after annealing for 0.2 ns, the $g_{\rm Ni-Ni}(r)$ features the shape commonly known for an amorphous phase, while the crystalline peaks of $g_{\rm Nb-Nb}(r)$ remain, indicating at this moment a Ni-rich amorphous alloy has been formed and coexists with some remaining Nb crystals. With increasing annealing time, the strength of the $g_{\rm Nb-Ni}(r)$ first peak increases and those peaks of the $g_{\rm Nb-Nb}(r)$ at long distances gradually disappear. After 0.5 ns, the Nb crystal becomes completely disordered and the four $g(r)$ curves apparently feature the shape for the amorphous alloys. From 0.5 ns-1.25 ns, a homogenizing process takes place and the composition of the amorphous alloy becomes more even. It is anticipated that after an adequate annealing time, the amorphous alloy would have a completely uniform composition.

The variation of the enthalpy and the volume of the model are calculated and shown in Figure 3. One sees that the enthalpy and volume increase before 0.024 ns due to the heating of the model up to the designed temperature and that the enthalpy is declining and the volume is relaxing to a stable state during isothermal annealing. These results suggest that the process of diffusion, alloying and amorphization is accompanied with a decrease of enthalpy, which is in agreement with a negative heat of formation of the Ni-Nb system calculated by Miedema's model [30]. Explicitly speaking, from a thermodynamic point of view, the free energy of the amorphous state is considerable more negative than that of the initial multilayers and the energy difference serves as a major driving force for SSA.

Besides, other sandwich-models combined with low-index atomic planes of Ni and Nb are constructed to study the interfacial reaction. For sandwich-models consisting of Nb (111), *i.e.* the most open plane of bcc metal, and any Ni atomic planes, SSA can take place spontaneously without a preset disordered interlayer. However for

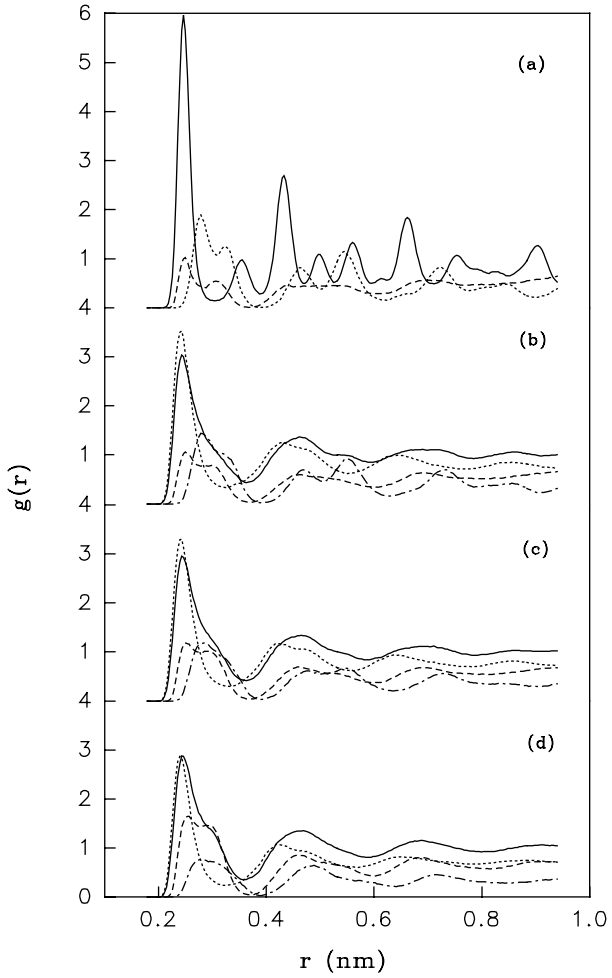

Fig. 2. Partial and total pair correlation functions for the initial state (a) and three further states obtained by annealing at 500 °C for (b) 0.2 ns, (c) 0.5 ns and (d) 1.25 ns, in the sandwich-model of [4 (001) Nb/8 (001) Ni/2 (001) Nb]. The solid line is for total $g(r)$; the short dashed line is for Nb-Ni $g(r)$; the dotted line is for Ni-Ni $g(r)$; and the dot-dashed line is for Nb-Nb $g(r)$.

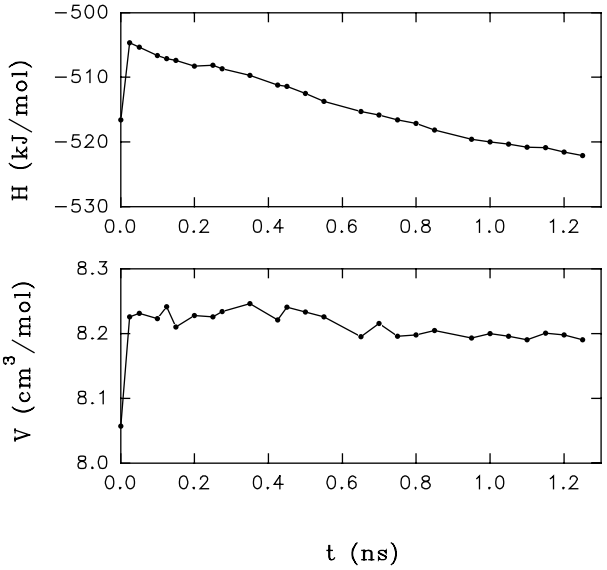

Fig. 3. The variation of the enthalpy and volume of the system *versus* time step of the sandwich-model of [4 (001) Nb/8 (001) Ni/2 (001) Nb] during isothermal annealing at 500 °C.

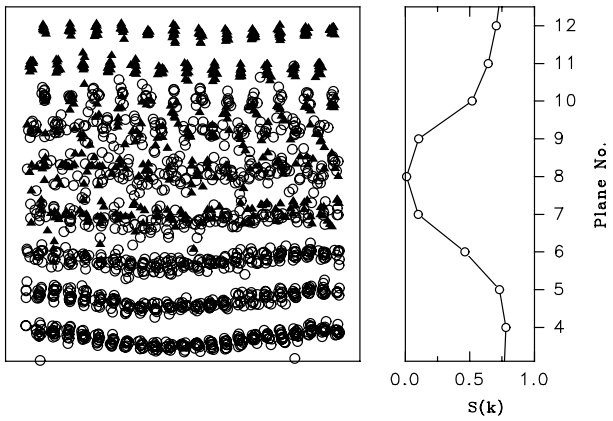

Fig. 4. A snapshot of the projection of the atomic positions on the x-z plane of the No. 4-12 atomic plane in the bilayer model [8 (001) Ni/8 (001) Nb] after annealing at 500 °C for 0.1 ns together with the corresponding planar structure factors $S(k)$: (◯) Ni; (▲) Nb.

sandwich-models consisting of Nb (001), it is necessary to induce some chemical disorder in the interfaces for SSA to proceed. For sandwich-models with close-packed planes Nb (110), SSA is hindered at an annealing temperature as high as 600 °C, even though the disordered interlayers are introduced by setting $\eta = 0$ in the interfaces. These results are similar as those observed in the Ni-Mo system [10].

4.2 Bilayer model

We now discuss the simulation results of a bilayer-model of [8 (001) Ni/8 (001) Nb] upon annealing. The interface separating the Ni and Nb lattices lies between atomic planes No. 8 and No. 9. A disordered interlayer is preset in the bilayer by randomly exchanging an equal number of Ni and Nb atoms in atomic planes No. 7-No. 10. After exchanging, the numbers of Ni and Nb atoms are 131 and 101 in plane No. 7, 163 and 79, 92 and 52, 88 and 56 in planes No. 8-10, respectively. The model is first pre-run at 27 °C to equilibrate for 25 ps and then heated up for isothermal annealing to 600 °C. Figure 4 displays a projection of the atomic positions on an y-z plane for No. 4-12 atomic planes with the corresponding planar structure factors $S(k)$ after annealing for 0.1 ns. One sees that although the Ni planes No. 7-8 and Nb planes No. 9-10 have all had chemical disordering imposed upon them, only three among the four, *i.e.* planes No. 7-9, have become amorphous as their planar structure factors are nearly zero. The composition of the amorphous phase is calculated to be 22.9 at.% Nb with Ni enrichment compared to the overall composition, *i.e.* 37.3 at.% Nb, of the bilayer. The No. 10 plane retains its bcc structure although 88 Nb atoms were

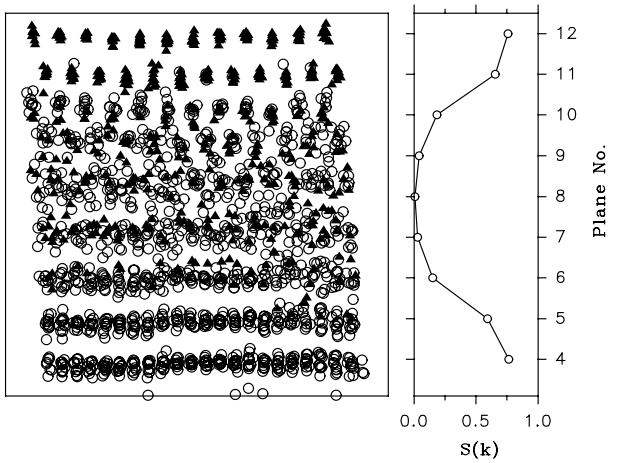

Fig. 5. A snapshot of the projection of the atomic positions on the x-z plane of the No. 4-12 atomic plane in the bilayer model [8 (001) Ni/8 (001) Nb] after annealing at 500 °C for 1.0 ns together with the corresponding planar structure factors $S(k)$: (◯) Ni; (▲) Nb.

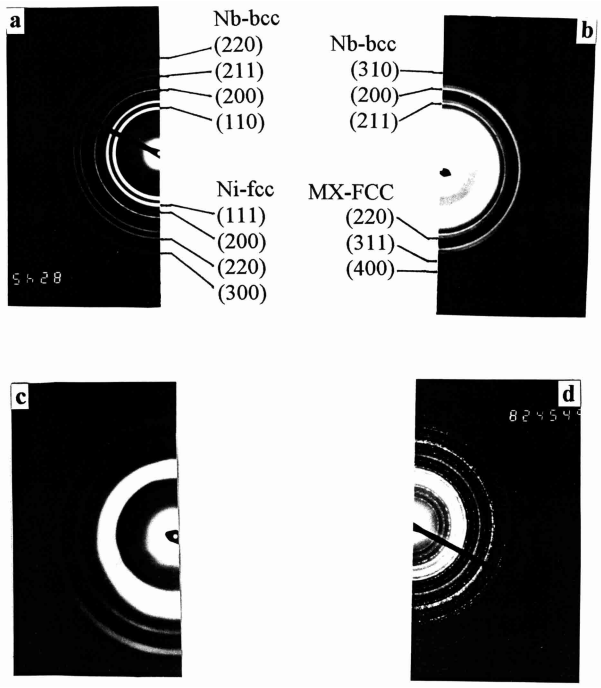

Fig. 6. Structural evolution of the $Ni_{48}Nb_{52}$ multilayered films at various stages of consecutive annealing at different temperatures as evidenced by the following selected area diffraction patterns (a) the initial-deposited state, (b) after annealing at 350 °C for 120 min, (c) after annealing at 400 °C for 60 min, and (d) after annealing at 550 °C for 30 min.

replaced by Ni atoms during presetting, suggesting the Nb lattice is very stable and capable of accommodating a number of Ni atoms as solutes. Figure 5 shows the calculated $S(k)$ values for the atomic planes No. 4-12 after further annealing up to 1.0 ns. It can be visualized that two atomic planes (*i.e.* No. 6 and 10) initially adjacent to the disordered interlayer become completely disordered by further mutual atomic diffusion, as their planar structure factors decrease from 0.62, and 0.50, respectively, down to about 0.1. At this moment, more Ni atoms have diffused into atomic plane No. 10 and the quantity of Ni atoms is 117, *i.e.* 29 Ni atoms have been added to the plane. Moreover, the pair-correlation function $g(r)$ is calculated for five atomic planes (No. 6-10) and confirms that this block of materials is of amorphous structure. The composition of this amorphous phase is increased to 28.4 at.% Nb, yet is still Ni-enriched compared with the overall composition of the bilayer model. The simulation time in this study is up to 3.0 ns and the $S(k)$ value of atomic plane No. 5 is found to decrease to 0.4 indicating a disorder tendency, while the $S(k)$ of No. 11 is as high as 0.68 suggesting a strong asymmetric growth behavior of the amorphous layer. It can be deduced that the amorphous layer grows to Ni and Nb lattices in a plane by plane mode during isothermal annealing and the average composition of the resultant amorphous phase is Ni enriched.

It is also found that the correlation of the thickness of the amorphous layer X towards the Ni side *versus* $t^{1/2}$ can be well fitted onto a straight line, indicating that the growth of the amorphous layer follows a diffusion-governed $t^{1/2}$ law, which is also compatible with our previous results [9,10].

5 Experimental evidence of asymmetric growth

The Ni/Nb multilayered samples were prepared by alternative deposition of pure nickel and niobium at a depositing rate of 0.5 Å/s onto cleaved NaCl single crystals in an ultra high vacuum (UHV) e-gun evaporation system with a vacuum level of 10^{-11} torr. The vacuum level during evaporation was better than 1.6×10^{-8} torr. No special cooling was provided for the substrates and the substrate temperature during evaporation was estimated to be below 200 °C. The total thickness of the films was designed to be about 500 Å and each sample consisted of five layers. After deposition, the composition of the Ni-Nb multilayered films was determined to be $Ni_{48}Nb_{52}$ by energy-dispersive spectrum (EDS) analysis within an experimental measuring error of 3%. The films were removed from the substrates by de-ionized water and placed on Cu grids. Solid state interfacial reaction was carried out in a hot- stage attached to a transmission electron microscope (TEM). The base vacuum level of the TEM was of the order of 10^{-7} torr. Selected area diffraction (SAD) was employed to take the diffraction patterns of the studied samples *in situ* at various annealing stages. The annealing is a consecutive procedure beginning at 250 °C rising 50 °C every 60 or 120 minutes eventually up to 550 °C.

Figure 6a shows a selected area diffraction (SAD) pattern of the initial deposited $Ni_{48}Nb_{52}$ multilayered films, confirming the crystalline structures of the Ni and Nb in

the initiate state. After annealing at 250 °C for 60 min, the sharp diffraction lines shown in Figure 6a, especially the strongest Ni (111) and Nb (110) diffraction lines, broaden, the weaker diffraction lines have disappeared. This suggests that solid-state interfacial reaction has taken place, though inter-diffusion was slow at 250 °C. After annealing at 350 °C for 120 min, a corresponding SAD pattern in Figure 6b shows clearly that a diffuse halo has appeared, located between the original Ni (111) and Nb (110) lines; all the Ni diffraction lines have disappeared, whereas some Nb diffraction lines still remain. In addition, some new diffraction lines have appeared that can be indexed to originate from a new metastable crystalline (MX) phase of FCC structure with $a_{\mathrm{fcc}} = 4.08$ Å. These results indicate that a Ni-Nb amorphous interlayer is formed in the interfacial region and that the Ni lattice has collapsed earlier than the Nb lattice. After further annealing at 400 °C for 60 min, almost all the crystalline lines from Nb and the FCC MX phase seen in Figure 6b have disappeared to be replaced by several diffuse halos reflected from a Ni-Nb amorphous phase as shown in Figure 6c. A close look at the pattern reveals that there is a very weak diffraction line remaining which is reflected from a trace amount of the FCC MX phase. According to our previous study, the FCC MX phase is of Nb-based solid solution formed through a two-step phase transition [21]. Consequently, the composition of the predominant Ni-Nb amorphous phase is slightly richer in Ni than the initial deposited sample. From Figures 6b and c, in the process of solid-state amorphization through interfacial reaction between the Ni and Nb layers, the Ni and Nb crystalline lattices collapse in a sequence corresponding to the asymmetric growth of the amorphous interlayer observed by MD simulation. The formed Ni-Nb amorphous phase remained unchanged after remaining at 450 °C for 60 min but eventually recrystallized and transformed into the γ phase when the sample was further annealed at 550 °C for approximately 30 min, as evidenced by the corresponding SAD pattern shown in Figure 6d. The above structural evolution in the $Ni_{48}Nb_{52}$ multilayered films can be summarized as follows,

$$\mathrm{Ni{+}Nb(multilayers)} \xrightarrow{250\,^{\circ}\mathrm{C},\,60\,\mathrm{min}} \mathrm{Ni{+}Nb} \xrightarrow{350\,^{\circ}\mathrm{C},\,60\,\mathrm{min}}$$

$$\mathrm{A{+}Nb{+}FCC} \xrightarrow{400\,^{\circ}\mathrm{C},\,120\,\mathrm{min}} \mathrm{A{+}trace\,of\,FCC} \xrightarrow{550\,^{\circ}\mathrm{C},\,30\,\mathrm{min}} \gamma$$

in which A represents amorphous phase, FCC is the MX phase.

6 Discussion

We now try to answer two questions. Firstly, why the solid solution can be regarded as the precursor of the amorphous phase. Secondly, what is the physical origin of the asymmetric growth observed both in experiments and MD simulations.

We construct the simulated solid solution models consisting of $8 \times 8 \times 6 \times 4 = 1536$ atoms for fcc Ni or $9 \times 9 \times 8 \times 2 = 1296$ atoms for bcc Nb crystals. In the two models, the [100], [010] and [001] atomic lattice directions are parallel to x, y and z axis, respectively, where periodic boundary conditions are adopted. Each desired solid solute concentration is obtained by randomly substituting a corresponding amount of Ni (Nb) with Nb (Ni) in the Ni fcc (Nb bcc) lattice. From the initial configuration, the model has a first equilibrating run at 27 °C for several time steps until all the relevant dynamic variables show no secular variation. Figure 7 displays the total and partial pair-correlation function $g(r)$ calculated after equilibrating for three Ni-rich fcc solid solutions with Nb solute concentrations of 10, 17 and 25 at.%, respectively. One sees that the solid solution with 10 at.% Nb retains fcc crystalline structure and that a crystal-to-amorphous transition apparently takes place in the solid solution with 25 at.% Nb, as the calculated $g(r)$ curves are of the shapes commonly observed for amorphous alloys. For the case of 17 at.% Nb, the shape of $g(r)$ is ambiguous, suggesting a glassy transition does take place but is not completed. On the Nb side, it is found that a similar, spontaneous decay of solid solution does not take place even at a solute concentration up to 50 at.% Ni.

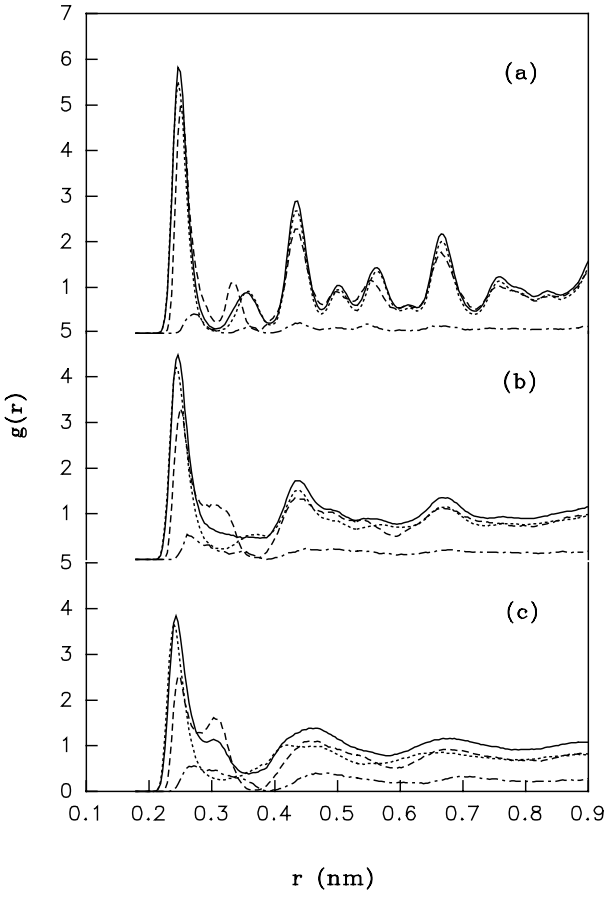

Fig. 7. Total and partial pair-correlation functions for the fcc Ni-rich solid solution of composition (a) 10%, (b) 17% and (c) 20% Nb after isothermal annealing at 27 °C. The solid line is for total $g(r)$; the short dashed line is for Nb-Ni $g(r)$; the dotted line is for Ni-Ni $g(r)$; and the dot-dashed line is for Nb-Nb $g(r)$.

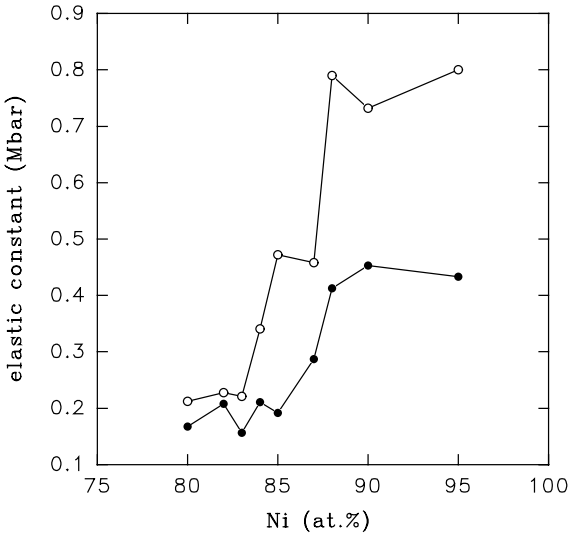

Fig. 8. Tetragonal shear modulus C' (filled circle) and rhombohedral C_{44} (open circle) *versus* compositions of Ni fcc solid solution after annealing at 27 °C. The solid lines are drawn for guidance.

The elastic constants of the Ni-based solid solutions are determined using the approach proposed by Parrinello and Rahman [31, 32]. Figure 8 displays the tetragonal shear modulus C' and rhombohedral shear modulus C_{44} *versus* the composition of the Ni fcc solid solution after annealing at room temperature. It can be seen that both shear moduli increase a little at first, which might be due to the rigidity of the dissolved Nb atom. Then a significant degree of moduli softening is observed in the composition range 13-15 at.% Nb, which is close to the critical value of 17 at.% Nb determined above by the pair correlation function calculation. The above results seem to suggest that the amorphization transition of the solid solution is probably triggered by mechanical instability.

Unlike the crystalline intermetallic compounds, nucleation of the solid solution is readily to proceed, since it requires no structural or chemical rearrangement. Therefore, mutual diffusion of atoms crossing the interfaces into the lattice of the partner metals results in the formation of solid solutions first. According to the above simulation, if the concentration of the solute atoms reaches a critical value, a spontaneous decay would take place. Due to the composition gradient, the crystal-to-amorphous transition will first occur at interfaces and a nucleus of amorphous phase is thus formed.

Accordingly, the reason for a sharp interface serving as a nucleation barrier can be clarified. Sharp interfaces prevent atoms from crossing-interface migrating, therefore insufficient solute atoms can diffuse into the solvent lattice to transform the original crystalline lattice into a disordered state, leading to no nucleation of the amorphous phase. Take the above mentioned sandwich-model [4 (001) Nb/8 (001) Ni/2 (001) Nb] as a typical example. There are 242 Ni atoms in one Ni (001) plane and 144 Nb atoms in one Nb (001) plane. At 27 °C, without the preset disordered interlayer, *i.e.* without a nucleus, the model possesses a total energy of −14 900 eV after equilibrating for 25 ps. However, providing a nucleus of amorphous phase by exchanging atoms in the interfaces, the total energy of the model is of −15 098 eV after equilibrating for 25 ps. The reduction of the total energy is from the negative heat of formation between the Ni and Nb atoms. If no nucleus is imposed, the diffusion and reaction are very slow, *e.g.* after annealing at 500 °C for 0.4 ns, only about 35 Ni atoms diffuse into the Nb lattice in one interface and even fewer Nb atoms diffuse into the Ni lattice. On the other hand, if chemical disorder is imposed on the interfaces (corresponding to $\eta = 0$), altogether 90 Ni and 90 Nb atoms should be exchanged in one interface. After exchanging, there are 54 Nb atoms plus 90 Ni atoms in No. 4 plane and 152 Ni atoms plus 90 Nb atoms in No. 5 plane. The degree of artificial alloying of two metal species is much larger than that resulting from spontaneous diffusion. In fact, such exchanging leads to the formation of a nucleus of amorphous phase at interfaces. Beginning with this configuration, annealing at 500 °C for 0.5 ns results in complete alloying of all the atoms.

Our simulation results also show that the critical concentration for Nb bcc solid solution is quite large, *i.e.* a large number of Ni solute atoms is necessary to make the bcc Nb solid solution become unstable and turn into an amorphous state. We therefore conclude that the Ni lattice undergoes an amorphous transition easier than the Nb lattice.

Based on the above results and those described in Section 4.1, SSA in the Ni-Nb multilayers upon isothermal annealing cab be understood as follows. Some Nb atoms diffuse into the Ni lattice and simultaneously some Ni atoms originally located at their fcc crystal lattice sites migrate into the preset amorphous interlayer. These two processes cause the Ni lattice to gradually become unstable; when the Nb concentration reaches the critical value, the Ni lattice decays into an amorphous state. Though these two processes also occur for the Nb lattice, the extension of the amorphous interlayer towards the Nb side proceeds at a much lower rate than that towards the Ni side, because the Nb lattice has a large capability of dissolving its partner Ni atoms. It follows that the physical origin of the asymmetric growth during SSA is related to the different capabilities of the constituent metal lattices in accommodating the partner atoms as solutes.

7 Conclusion

1. We have constructed a realistic n-body Ni-Nb potential based on the embedded-atom method. This has the potential to reproduce some documented physical properties, as well as to reveal through MD simulation, the details of solid-state interfacial reaction in the Ni-Nb multilayers, which are compatible with experimental observations.
2. Our simulation results show that solid-state amorphization proceeds by mutual crossing- interface atomic diffusion, alloying between layers, nucleation of amorphous layer(s) at interface(s) and a subsequent

growth of the amorphous interlayer(s) expanding into both Ni and Nb sides. The nucleation of the amorphous phase is from the spontaneous decay of the solid solutions, which can be regarded as the precursor of amorphization.

3. The growing speed of the amorphous interlayer towards the Ni lattice is found to be faster than that directed to the Nb side and such asymmetric growth behavior can be attributed to the difference of the solid solubilities of the constituent metals. Moreover, the simulation results are compatible with our experimental investigations.

This study is supported by the National Natural Science Foundation of China. Partial financial aid from the Tsinghua Administration is also gratefully acknowledged.

References

1. R.B. Schwarz, W.L. Johnson, Phys. Rev. Lett. **51**, 415 (1983).
2. M. van Rossum, M.-A. Nicolet, W.L. Johnson, Phys. Rev. B **29**, 5498 (1984).
3. B.M. Clemens, Phys. Rev. B **33**, 7615 (1986).
4. K. Samwer, H.J. Fecht, W.L. Johnson, *Glassy Metals III: Amorphization Techniques, Catalysis, Electronic and Ionic structure*, edited by H. Beck, H.J. Güntherodt (Springer-Verlag, Berlin, 1995).
5. A.M. Vredenberg, J.F.M. Westendorp, F.W. Saris, N.M. van den Pers, T.H. de Kedser, J. Mater. Res. **1**, 774, (1986).
6. R.J. Highmore, Philos. Mag. B **62**, 455 (1990).
7. W.J. Meng, Ph.D. Thesis, Dept. of Applied Physics Calif. Inst. of Tech.
8. H. Schröder, K. Samwer, U. Koster, Phys. Rev. Lett. **54**, 197 (1985).
9. W.S. Lai, B.X. Liu, Phys. Rev. B **58**, 6063 (1998).
10. Q. Zhang, W.S. Lai, B.X. Liu, Phys. Rev. B **58**, 14020 (1998).
11. G. Kreuch, J. Hafner, J. Non-Cryst. Solids **189**, 227 (1995).
12. M.S. Daw, I. Baskes, Phys. Rev. Lett. **50**, 1285 (1983).
13. R.A. Johnson, Phys. Rev. B **37**, 3924 (1989).
14. V. Rosato, M. Guillope, B. Legrand, Philos. Mag. A **59**, 321 (1989).
15. M.W. Finnis, J.E. Sinclair, Philos. Mag. A **50**, 45 (1984).
16. J.H. Rose, J.R. Smith, F. Guinea, J. Ferrante, Phys. Rev. B **29**, 2963 (1984).
17. R.A. Johnson, D.J. Oh, J. Mater. Res. **4**, 1195 (1989).
18. J. Cai, Y.Y. Ye, Phys. Rev. B **54**, 8398 (1997).
19. R.A. Johnson, Phys. Rev. B **41**, 9717 (1990).
20. X.Y. Huang, J.S. Pan, Y.D. Fan, Solid State Commun. **104**, 101 (1997).
21. Z.J. Zhang, H.Y. Bai, Q.L. Qiu, T. Yang, K. Tao, B.X. Liu, J. Appl. Phys. **73**, 1702 (1993).
22. Z.J. Zhang, B.X. Liu, J. Appl. Phys. **75**, 4948 (1994).
23. Joint Committee on Powder Diffraction Standards (JCPDS), Card No. 15-0101.
24. E.A. Brandes, G.B. Brook, *Smithells Metals Reference Book*, 7th edn. (Butterworth-Heinemann, Oxford, 1992).
25. M. Parrinello, A. Rahman, J. Appl. Phys. **52**, 7182 (1981).
26. Y. Waseda, *The Structure of Non-Crystalline Materials; Liquids and Amorphous Solids* (McGraw-Hill, New York, 1980).
27. S.R. Phillpot, S. Yip, D. Wolf, Comput. Phys. **3**, 20 (1989).
28. V. Rosato, G. Ciccotti, V. Pontikis, Phys. Rev. B **33**, 1860 (1986).
29. C. Massobrio, V. Pontikis, G. Martin, Phys. Rev. B **41**, 10486 (1990).
30. F.R. de Boer, R. Boom, W.C. M. Matters, A.R. Miedema, A.K. Niessen, *Cohesion in Metals: Transition Metal Alloys* (North-Holland, Amsterdam, 1988).
31. M. Parrinello, A. Rahman, J. Appl. Phys. **52**, 7182 (1981).
32. M. Parrinello, A. Rahman, J. Chem. Phys. **76**, 2662 (1982).